



1 **Inland lake temperature initialization via cycling with atmospheric data**
2 **assimilation**

3
4 Stanley G. Benjamin¹, Tatiana G. Smirnova^{2,1}, Eric P. James^{2,1}, Eric J. Anderson³,
5 Ayumi Fujisaki-Manome^{4,5}, John G.W. Kelley⁶, Greg E. Mann⁷, Andrew D. Gronewold⁵
6 Philip Chu⁸, Sean G.T. Kelley⁹

7
8 ¹NOAA Global Systems Laboratory, Boulder, CO 80305 USA

9 ²Cooperative Institute for Research in Environmental Science (CIRES), University of
10 Colorado, Boulder, CO 80303 USA

11 ³Civil and Engineering Department, Colorado School of Mines, Golden, CO USA

12 ⁴Cooperative Institute for Great Lakes Research (CIGLR), University of Michigan, Ann
13 Arbor, MI USA

14 ⁵University of Michigan, Ann Arbor, MI USA

15 ⁶NOAA National Ocean Service, Coast Survey Development Laboratory, Durham,
16 NH 03824 USA

17 ⁷NOAA National Weather Service, White Lake, MI, USA

18 ⁸NOAA Great Lakes Environmental Research Laboratory, Ann Arbor, MI, USA

19 ⁹University of Massachusetts, Department of Mathematics and Statistics,
20 Amherst, MA, USA

21

22 *Correspondence to:* Stan Benjamin (stan.benjamin@noaa.gov)

23

24

25

26

27

28

29

30 **Abstract.** Application of lake models coupled within earth-system prediction models,
31 especially for short-term predictions from days to weeks, requires accurate initialization
32 of lake temperatures. Here, we describe a lake initialization method by cycling within
33 an hourly updated weather prediction model to constrain lake temperature evolution.
34 We compare these simulated lake temperature values with other estimates from
35 satellite and in situ and interpolated-SST data sets for a multi-month period in 2021.
36 The lake cycling initialization, now applied to two operational US NOAA weather
37 models, was found to decrease errors in lake temperature from as much as 5-10K
38 (using interpolated-SST data) to about 1-2 K (comparing with available in situ and
39 satellite observations).

40

41 **Short summary**

42

43 Application of 1-d lake models coupled within earth-system prediction models will
44 improve accuracy but requires accurate initialization of lake temperatures. Here, we



45 describe a lake initialization method by cycling within a weather prediction model to
46 constrain lake temperature evolution. We compare these lake temperature values with
47 other estimates and found much reduced errors (down to 1-2 K). The lake cycling
48 initialization is now applied to two operational US NOAA weather models.

49

50 **1 Introduction**

51

52 Inclusion of lake representation into numerical weather prediction (NWP) models has
53 become increasingly necessary to further improve representation of atmosphere-
54 surface fluxes of heat and moisture as model grid resolution becomes finer.
55 Representation of lake physics to provide time-varying lake surface properties (e.g.,
56 Subin et al, 2012) is essential to improve fluxes of heat, moisture and momentum
57 between the surface and atmosphere (Hostetler et al, 1993, Thiery et al, 2014). Lake
58 representation is part of the overall surface treatment including land-surface models
59 (LSMs) necessary to accurately model the evolution of the planetary boundary layer.
60 Lakes are estimated to cover 3.7% of the global non-glaciated land area (Verpoorter et
61 al, 2014), and they significantly moderate sensible heat and moisture fluxes from this
62 'land' (i.e., non-ocean) area. Water impoundments (reservoirs) that used to account for
63 about 6% of these 'lake' areas (Downing et al, 2006) have recently increased to 9%
64 (Vanderkelen et al, 2021). Initial conditions for both land and lake surface are an
65 important consideration due to far larger thermal inertia for soil or water than for air.
66 Consequently, incorrect soil or lake initial conditions can result in erroneous heat and
67 moisture fluxes that may persist for days and even weeks (e.g., Dirmeyer et al, 2018).
68 This potential source of error in fluxes is more pronounced for lake areas with far larger
69 thermal inertia and heat storage than even saturated soils.

70

71 In the US, operational NWP models have used coarse-resolution daily SST analyses to
72 specify the surface water temperatures for the ocean and the Laurentian Great Lakes
73 for the entire forecast period. However, given the resolution, the temperatures for bays,
74 sounds, and smaller non-Great Lakes have been obtained by the interpolation of values
75 from the ocean and the Great Lakes. An alternative is to incorporate one-dimensional
76 (1-d) lake models within NWP models.

77

78 Lake representation (via one-dimensional (1-d) models, as in LSMs) within NWP
79 models is beneficial by providing a first-order accurate lagged effect of the seasonal
80 variation in temperature, with lake water remaining colder than nearby land in spring
81 and warmer in autumn. The outcomes are desirable, as described by Balsamo et al,
82 (2012), for instance by accurately representing increased evaporative fluxes in the fall.
83 Thus, use of a 1-d lake model improves over land representation by capturing this
84 slower seasonal response.

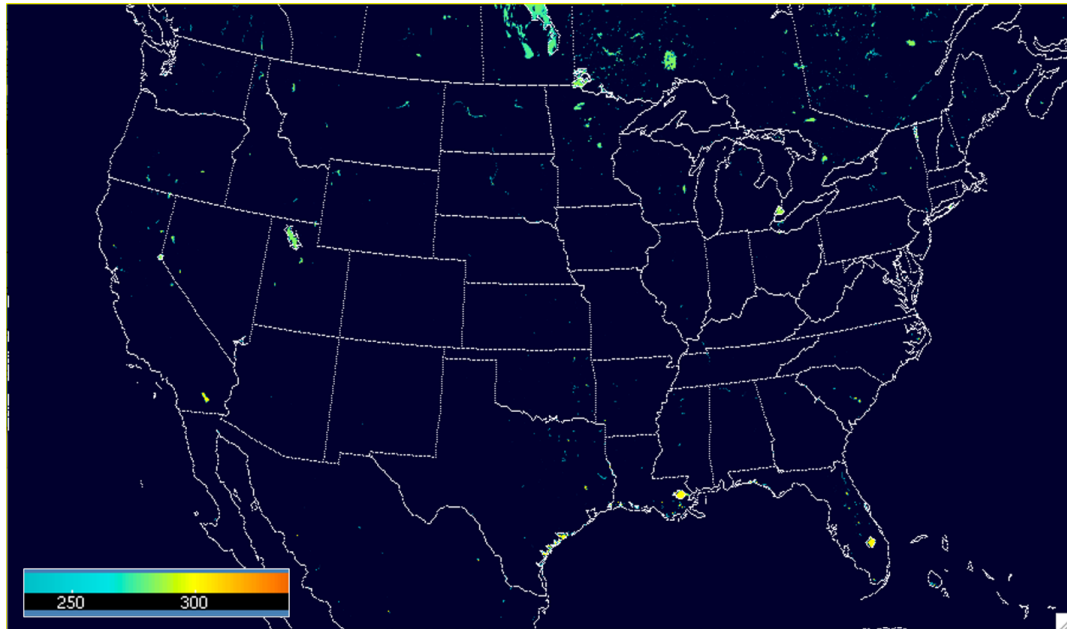
85

86 However, lake temperature initialization is still a problem. Use of spatial interpolation to
87 smaller lakes from larger (and deeper) lakes, or from the ocean, for lake initialization
88 (e.g., Mallard et al, 2015) can exaggerate this seasonal slower response. Shallow lakes

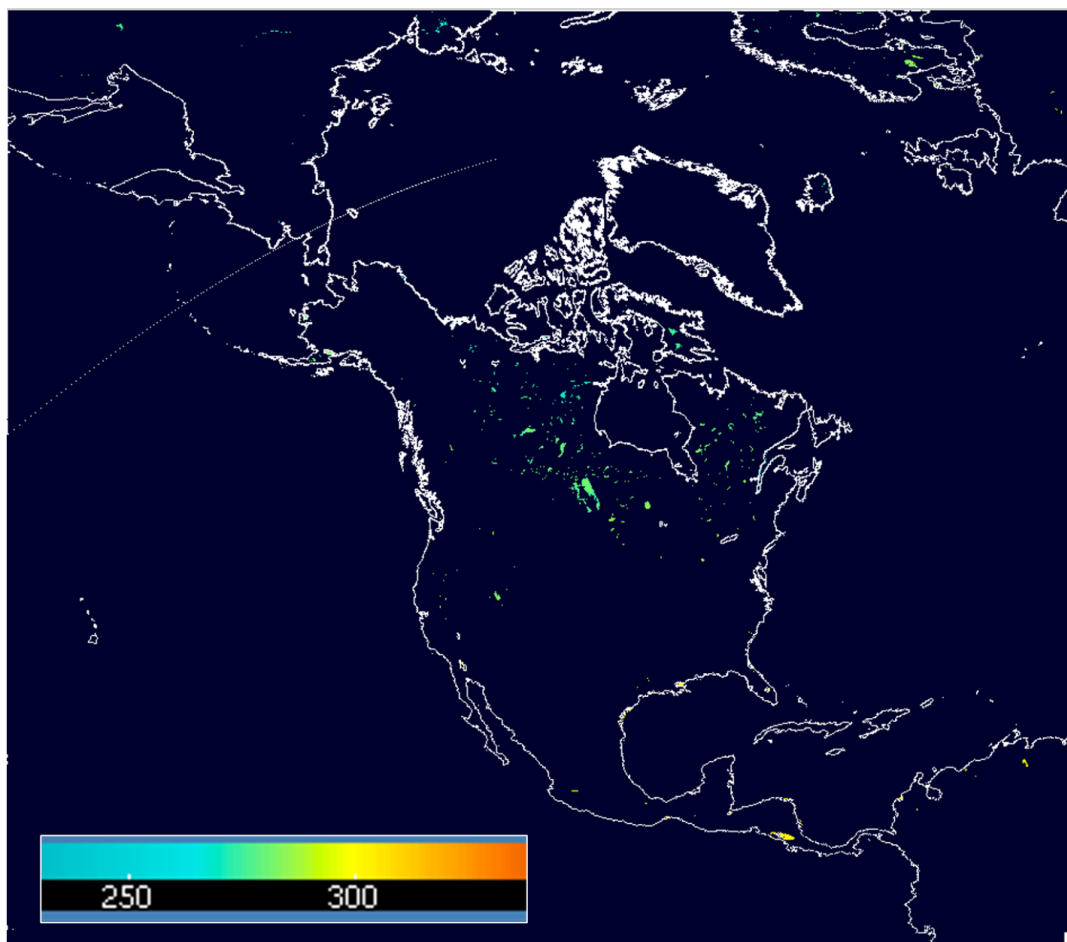


89 warm more slowly in spring than surrounding land, but more quickly than nearby deeper
90 lakes. Even in summer, it will take at least 1-2 weeks for 1-d models to adjust from
91 values interpolated from deeper-lake temperatures to become more realistic for shallow
92 lakes. Therefore, lake temperature initialization becomes the most important factor to
93 accurately simulate sensible and latent heat fluxes from lakes for short to medium-range
94 NWP, more so than the use of the lake model itself. One option to solve the lake
95 initialization problem is to use a model-based climatology for seasonal variation of lake
96 temperatures (Balsamo et al (2012) and Balsamo (2013)) using a 1-d lake model forced
97 by reanalysis data. This technique avoids a new spin-up with each new run, but cannot
98 capture unique weather regime variations in a given region and time. Another option,
99 described here, is lake cycling, a cost-free option if the atmospheric conditions are
100 relatively accurate.

101
102 Data assimilation for land-surface fields (e.g., soil temperature, soil moisture, snow
103 cover, snow water equivalent, snow temperature) has been very beneficial for improved
104 short-range weather prediction accuracy (e.g., Balsamo and Mahfouf, 2020, Muñoz-
105 Sabater et al, 2019, Benjamin et al, 2022, others), but lake temperature has not been a
106 part of this surface data assimilation. In December 2020, the NOAA 13-km Rapid
107 Refresh (RAP) and 3-km High-Resolution Rapid Refresh (HRRR) implemented an
108 interactive small-lake multi-layer 1-d lake model, the first NOAA weather models to do
109 so. The lake coverages for the HRRR and RAP models are shown in Fig. 1. The
110 weather models are coupled with the 10-layer Community Land Model (CLM) version
111 4.5 lake model, (Subin et al, 2012, Mallard et al, 2015), an option within the community
112 Weather Research and Forecast model (WRF, Skamarock et al, 2019). The CLM lake
113 model is a 1-d thermal diffusion model allowing 2-way coupling with the atmosphere.
114 ECMWF had taken a similar approach earlier to improve their overall surface modeling
115 treatment by implementing the 2-layer FLake (Freshwater Lake Model) model (Mironov
116 et al, 2010, Balsamo et al, 2012, Boussetta et al, 2021) into their Integrated Forecast
117 System (IFS) in 2015. To initialize small-lake temperatures in the RAP and HRRR, all
118 lake variables have been evolving since summer 2018 depending on the cycled
119 atmospheric conditions and the lake model physics as discussed in section 4. The 1-d
120 lake model cannot represent 3-d hydrodynamical processes in larger bodies of water.
121 Thus, a second major improvement in 2020 with lake representation in the NOAA 3-km
122 HRRR model occurred with the implementation of lagged data coupling with the 3-d
123 hydrodynamic-ice model for the Laurentian Great Lakes as described by Fujisaki-
124 Manome et al (2020).



125
126 *Fig. 1a. Small-lake (green to yellow) areas for the a) 3-km HRRR domain using the*
127 *MODIS 0.15" resolution data for land/water and lake information. Color corresponds to*
128 *top-level lake temperature (K) at 01z 15 Oct 2019. Only small-lake areas treated in*
129 *HRRR by the CLM lake model are shown. Out of the 1,900,000 grid points in this*
130 *HRRR CONUS domain, 12,305 of them (~0.6%) are for small lakes (excluding the 5*
131 *Laurentian Great Lakes treated by separate coupling as described in text).*
132



133

134 *Fig. 1b. Same as Fig. 1a but for the 13-km RAP domain*

135

136

137 Here, we describe the design and results of a unique approach to inland small lake
138 initialization by cycling with hourly updating of atmospheric conditions (clouds/radiation,
139 near-surface temperature/moisture/winds). This lake initialization via cycling is an
140 important component of earth-system coupled modeling for effective NWP, with goals to
141 improve prediction of 2-m (air) temperature and moisture, cloud, boundary-layer
142 conditions, and precipitation for situational awareness enabling short-range decision
143 making (e.g., aviation, severe weather, hydrology, energy).

144

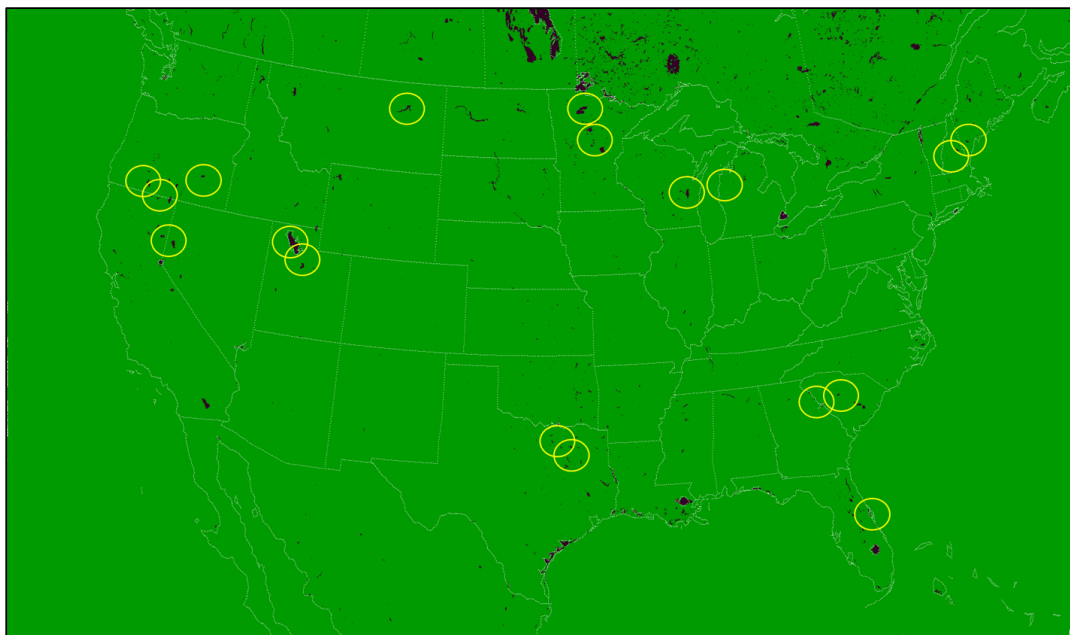
145 **2 Problem**

146

147 For the NOAA hourly updated mesoscale models, used frequently for short-range
148 weather prediction, poor 2-m air temperature and/or dewpoint forecasts have been
149 reported on many occasions by the US National Weather Service (NWS) in the vicinity



150 of inland lakes (Fig. 2). These hourly updated models included the Rapid Update Cycle
151 (RUC, Benjamin et al 2004) with horizontal grid spacing decreasing from 40-km to 20-
152 km to 13-km (Benjamin et al 2010), succeeded by the 13-km Rapid Refresh (RAP) and
153 3-km High-Resolution Rapid Refresh (HRRR, Benjamin et al, 2016, Dowell et al, 2022,
154 James et al, 2022). Many of these reported systematic deficiencies from the US NWS
155 were for the 2.5-km NOAA Real-Time Mesoscale Analysis (RTMA, Pondeca et al.
156 2011), using 1-h forecasts from the 3-km HRRR as a background. The most common
157 report was too-low 2-m air temperatures near inland lakes in late spring and summer.
158 At times, spurious prediction of fog formation was also noted on or near small lakes due
159 to erroneous lake temperatures and resultant fluxes.
160



161
162
163
164
165
166
167

Fig. 2. Lakes (here, in black) circled for those with related problem reports from US National Weather Service Forecast Offices on nearby deficient 2-m air temperature or dewpoint forecasts in NOAA hourly updated models during 2004-2019.

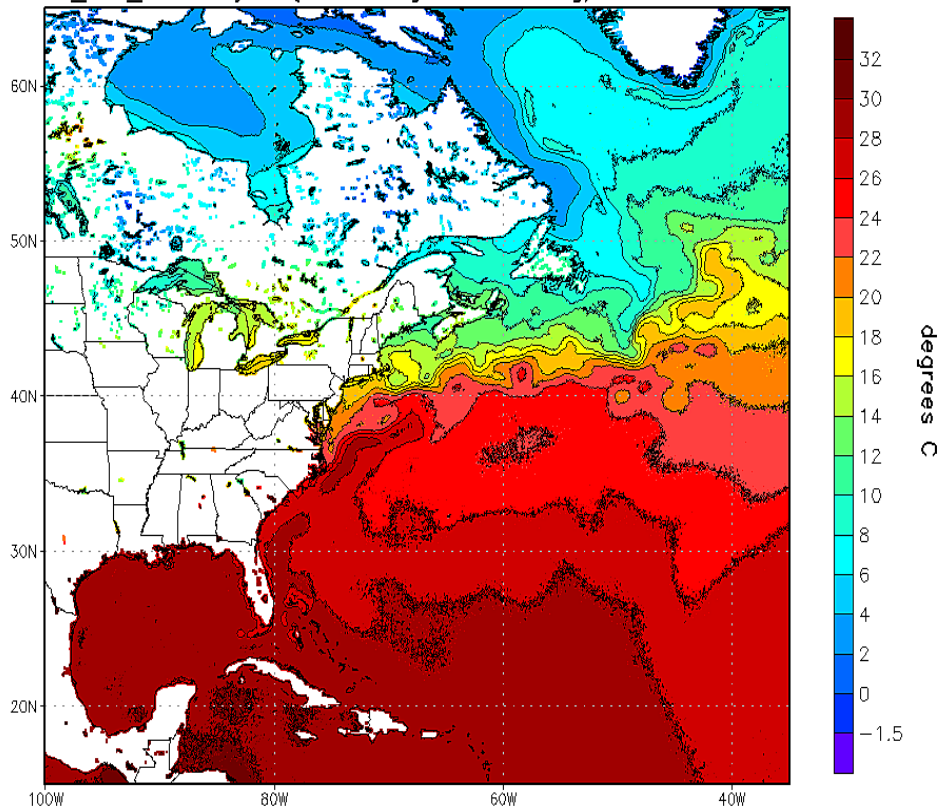
168 Further investigation revealed the water temperatures for small lakes used in NOAA
169 weather models were assigned via horizontal interpolation from larger, deeper bodies of
170 water (with available AVHRR data) in the design for the NOAA real-time gridded SST
171 analysis (RTG_SST_HR, Gemmill et al, 2007). An example of the analysis is shown in
172 Fig. 3. Temperature for the larger, deeper water areas has a lesser and more lagged
173 seasonal variation than the smaller, shallower lake areas due to their large heat storage
174 capacity. So use of the NOAA SST fields for lake temperatures resulted in generally
175 too-low values through spring and summer, and even into autumn. In situations with



176 atmospheric cold outbreaks in the autumn, shallow lake temperatures quickly decrease
177 (as reflected with lake cycling) and SST-based estimated lake temperatures were too
178 high. This behavior was consistent with the HRRR and RTMA deficiencies noted by
179 forecasters. In February 2020, NOAA changed from the RTG_SST_HR to a Near-
180 Surface Sea Temperature (NSST, see NWS, 2020) for SSTs, but using the same
181 horizontal interpolation method to estimate small-lake temperatures resulting in the
182 same temperature biases for small lakes.
183

NOAA/NWS/NCEP/EMC Marine Modeling and Analysis Branch Oper H.R.

RTG_SST_HR Analysis (0.083 deg X 0.083 deg) for 09 Oct 2019



184 22:40:13 WED OCT 9 2019

185

186 *Fig. 3. An example of small-lake temperatures spatially interpolated from deeper-water*
187 *temperature data in the NOAA SST analysis (Gemmill et al, 2007). For 9 October*
188 *2019, provided by NOAA National Weather Service.*

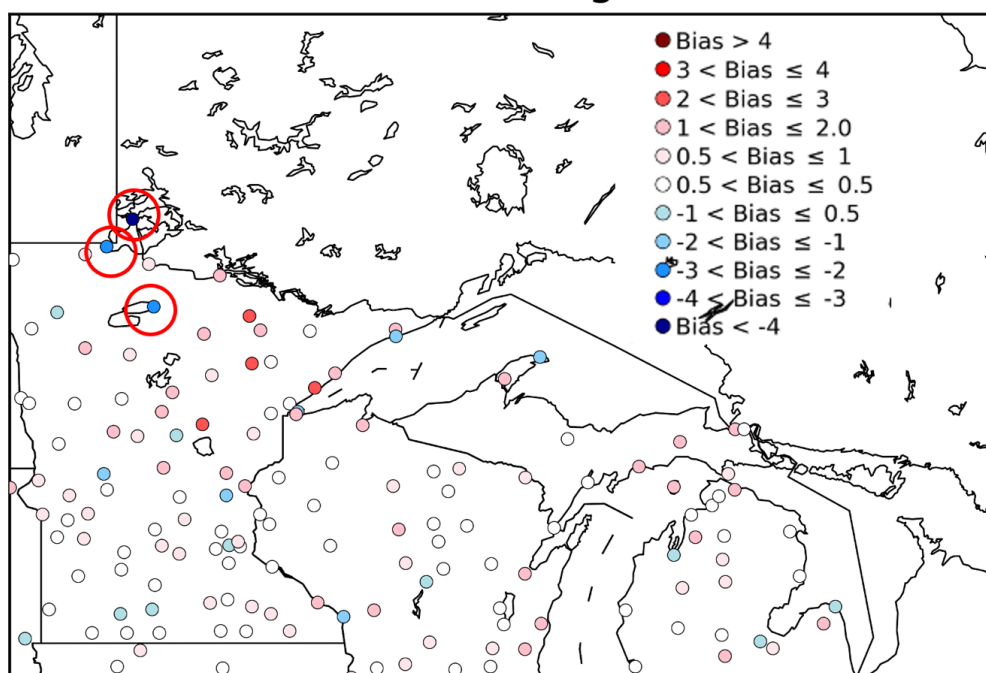
189

190 Hamill (2020), in a comparison benchmarking a statistical method for 2-m temperature
191 (at 00 UTC), showed the same problem with large summer temperature biases from the
192 HRRR 1-h forecasts in August 2018 especially in the vicinity of lakes (his Figs. 10, 11).



193 His results are shown in Fig. 4, with three stations showing coldest biases (at 00 UTC)
194 greater than 2 K (circled in red), all adjacent to lakes. In Fig. 4, these circled stations,
195 from north to south, are KFGN (Flag Island on Lake of the Woods; >3 K cold bias),
196 KRRT - Warroad, MN (west of Lake of the Woods), and KVVU – Waskish, MN (east of
197 Red Lake)). The overall warm or cold biases are generally < 2 K, but these stations
198 adjacent to lakes are outliers, consistent with introduction of cold-biased lake
199 temperatures through the NSST.

HRRR bias, August 2018



200
201 *Figure 4. 2-m temperature biases for 1-h HRRR forecasts valid at 00 UTC in August*
202 *2018 (from HRRRv3, before introduction of lake cycling and using NSST estimates*
203 *instead). Stations with low bias < -2 K are circled in red. (Credit and thanks to Thomas*
204 *Hamill, providing a regional version of his Fig. 10b in Hamill, 2020).*

205
206

207 With its 3-km grid spacing, the HRRR model can resolve many inland lakes (Fig. 1a).
208 Specification of surface temperatures for these small lakes using the horizontal
209 interpolation from the NOAA SST fields was problematic being determined by
210 interpolation from large lake and ocean temperatures.

211

212 In summary, errors in specified lake temperatures (as well as ice cover and
213 concentration) due to spatial interpolation from oceans and larger lakes can lead to
214 degraded atmospheric predictions in the vicinity of lakes. For small lakes, poor short-



215 range 2-m temperature (T) and 2-m dew point temperature (T_d) forecasts were noted in
216 vicinity of lakes, especially from spring through summer and into autumn. Specifically,
217 fluxes from lakes were often poorly estimated due to inaccurate lake temperature fields.
218

219 **3 Lake model for coupling with NOAA regional atmospheric models**

220
221 Similar to the now-commonplace (in NWP models) coupling with land-surface models
222 (LSMs) to improve fluxes into the atmosphere, a multi-level 1-d lake model was
223 implemented within the operational 3-km HRRR and 13-km RAP weather models in
224 December 2020, an extension to atmosphere-surface coupling. An effective lake
225 initialization is a necessary complement for the lake model coupling, as described in
226 section 4. Different earth-system coupling processes represented in the HRRR and
227 RAP models are described in Table 1, including land, snow, ice, and smoke. The
228 Community Land Model (CLM) lake model (same in versions 4.5 and 5.0) was added
229 for smaller lakes as an option in the WRF model version 3.6 (Mallard et al, 2015). The
230 CLM lake model is described in more detail below with its configuration for the NOAA
231 HRRR and RAP weather models. A detailed description of the physical processes
232 (cloud microphysics, turbulent exchange, land-surface, etc.) in the HRRR and RAP
233 models are described by Dowell et al (2022) and Benjamin et al (2016).



Component	Prognostic variables	Layers (below surface except for smoke)	Year introduced for experimental cycling	Year intro for NCEP	Data assimilation	Other information, references
Soil	Temp, moisture	9	1996 (6 levels until 2012)	1998 (6 levels until 2014)	Cycling, atmos-to-soil coupled DA	Moderately coupled DA (Benjamin et al 2022)
Snow	Water equiv, snow depth, temp	2	1997	1998	Cycling, atmos-to-snow DA for temp, trim/build from sat for cover	Moderately coupled DA. Subgrid fraction intro 2020
Ice	Temp	9	2010 (6 levels until 2012)	2012 (6 levels until 2014)	Cycling, atmos-to-surface coupled DA	Subgrid fraction intro 2018
Smoke	Smoke mixing ratio	50 atmos layers	2016	2020	Cycling, fire rad power from sat	No direct DA, only cycling
Small lakes	Temp, ice fraction, mixing	10	2018	2020	Cycling	No direct DA, only cycling
Large lakes (Great Lakes)	Temp, ice fraction, mixing	FVCOM levels	2018	2020	Independent	FVCOM driven by HRRR wind, rad, temp, 6h lag (Fujisaki-Manome et al 2020)

234

235

236 *Table 1. Earth-system coupling added to NOAA regional models (HRRR, RAP, RUC*
 237 *(pre-2012))*

238

239 An additional improvement in lake-atmosphere coupling in NOAA weather models was
 240 recently introduced, a coupling between the NOAA HRRR model using predicted lake
 241 temperatures and ice concentration fields from the NOAA GLERL/NOS 3-dimensional
 242 hydrodynamic-ice model run in real time over the Laurentian Great Lakes, as described
 243 by Fujisaki-Manome et al (2020). This hydrodynamic-ice model is based on the Finite
 244 Volume Community Ocean Model (FVCOM, Chen et al., 2006, 2013) coupled with the
 245 unstructured grid version of Los Alamos Sea Ice Model (CICE; Gao et al., 2011) and is
 246 applied to the Great Lakes Operational Forecast System (GLOFS, Anderson et al.,
 247 2018). This time-lagged data coupling (alternate applications of HRRR atmospheric
 248 forcing and FVCOM-CICE lake forcing about 6-12 h in advance) was incorporated to
 249 improve lake-effect snow (LES) predictions in winter but has also been found to improve
 250 near-lake atmospheric predictions year-round especially for upwelling events in the
 251 warm season. The use of FVCOM-CICE to specify lake temperatures addresses



252 previous errors in SST from relatively fast changes in lake temperatures due to cold air
 253 outbreaks or upwelling events. These changes sometimes escape AVHRR-derived SST
 254 detection due to multi-day cloud obscuration.
 255

Small lake size (grid points)	# Lakes	% of # of small lakes	% of small lake surface coverage	Avg depth (m)	Surface area of lakes (km ²)	Volume of lakes (km ³)
1 grid point (3kmx3km)	917	49%	7%	13	8,812	115
2 (~20 km ²)	323	17%	5%	12	6,208	76
3	155	8%	4%	11	4,468	49
4-5	157	8%	6%	14	6,746	97
6-10 (~100 km ²)	155	8%	10%	14	11,570	162
11-100 (~1000 km ²)	141	7%	30%	21	35,518	769
>100	16	<1%	38%	14	44,926	614
All	1864	100%	100%		118,248	1,882

256 *Table 2. Characteristics of small lakes (not including the five Laurentian Great Lakes)*
 257 *resolved in the 3-km HRRR CONUS domain over the lower 48 United States and*
 258 *adjacent areas of Canada and Mexico. Grid points were assigned as having a lake land*
 259 *use for points with at least 50% lake representation from the higher-resolution 15"*
 260 *MODIS land-use data.*
 261

Laurentian Great Lakes	Surface area of lakes (km²)	Volume of lakes (km³)
Superior	82,100	12,000
Michigan	57,800	4,920
Huron	59,600	3,540
Erie	25,670	484
Ontario	19,010	1,640

262
 263 *Table 3. Characteristics of the five Laurentian Great Lakes (surface area, volume)*
 264 *(Hunter et al 2015).*
 265



266

267

268 3.1 CLM lake model applied to HRRR for smaller inland lakes

269

270 Subin et al (2012) describe the 1-d CLM lake model as applied within the Community
271 Earth System Model (CESM) as a component of the overall CESM CLM (Lawrence et al
272 2019). Gu et al (2015) describe the introduction of the CLM lake model into the WRF
273 model and initial experiments using its 1-d solution for both Lakes Superior (average
274 depth of 147 m) and Erie (average depth of 19 m). The CLM lake model divides the
275 vertical lake profile into 10 layers driven by wind-driven eddies. The atmospheric inputs
276 into the model are temperature, water vapor, horizontal wind components from the
277 lowest atmospheric level and short-wave and longwave radiative fluxes (from the HRRR
278 model in this application). The CLM lake model then provides latent heat and sensible
279 heat fluxes back to the HRRR. The CLM lake model is called every 20 s within the
280 HRRR model. The CLM lake model was configured with the top layer fixed to a 10-cm
281 thickness (Gu et al 2015) and with the rest of the lake depth divided evenly into the
282 other 9 layers. Energy transfer (heat and kinetic energy) occurs between lake layers via
283 eddy and molecular diffusion as a function of the vertical temperature gradient. The
284 version of the CLM lake model used for HRRR and RAP was introduced with CLM
285 version 4.5 and continues without change in CLM version 5 (Lawrence et al, 2019). The
286 CLM lake model also uses a 10-layer soil model beneath the lake, a multi-layer ice
287 formation model and up to 5-layer snow-on-ice model (Gu et al, 2015). Testing of the
288 CLM lake model by the authors within WRF showed computational efficiency of the
289 model with no change of even 0.1% in run time with the HRRR and RAP applications.
290 Multiple layers in lake models better represent vertical mixing processes in the lake. By
291 intention, the CLM lake model was only applied for HRRR and RAP model to smaller
292 lakes, since NOAA began at the same time to provide temperature and ice cover
293 through GLOFS for the Laurentian Great Lakes through the 3-d hydrodynamic-ice
294 model (Fujisaki-Manome et al, 2020, Anderson et al, 2018).

295

296 3.2 Lake area mask

297

298 Grid points were assigned as lake points when the fraction of lake coverage in the grid
299 cell (derived from yet finer 15" MODIS data) exceeds 50% and when HRRR gridpoint
300 elevation > 5 m above sea level (to distinguish from ocean). The lake water mask is
301 therefore binary, set to either 1 or 0. This binary approach at 3 km seemed capable of
302 capturing the effect of lakes on regional heat and moisture fluxes. The alternative
303 subgrid lake fraction approach was used by ECMWF with their 9-km model (Choulga et
304 al, 2019).

305

306 An overview of the lake number, areal coverage, and integrated volume for the 3-km
307 HRRR model are depicted in Table 2. The HRRR CONUS domain (Fig. 1a) is able to
308 represent 1864 separate lakes occupying 0.6% of the entire domain. These water
309 bodies represented in HRRR as "lakes" include reservoirs and larger rivers, and about



310 half of the 1864 lakes are single-gridpoint lakes. The sixteen largest lakes in the HRRR
311 CONUS domain have surface area greater than 1,000 km², nine in Canada and two on
312 the US-Canada border (Lake of the Woods and Lake St. Clair). In contrast, the five
313 Laurentian Great Lakes (Table 3) range in size from 82,000 km² (Superior) to 19,000
314 km² (Ontario), and therefore, their representation in the coupled HRRR system (Table 1)
315 is handled with 3-d hydrodynamic-ice models (Fujisaki-Manome et al, 2020).

316

317 The lake area mask for the 3-km HRRR used an algorithm for identifying an ocean area
318 mask for all areas with contiguous water areas and leaving other areas as near-ocean
319 lagoon regions treated as lakes with the CLM 1-d lake model. These lagoon areas
320 separated from ocean by barrier islands in the HRRR representation (Fig. 1a) include
321 the Intracoastal Waterway in Texas largely separated from the Gulf of Mexico by Padre
322 Island, Indian River in Florida largely separated from the Atlantic Ocean by Merritt
323 Island, and Lake Pontchartrain in Louisiana. This ocean-contiguity technique is similar
324 to the flood-filling technique used by ECMWF (Choulga et al, 2019).

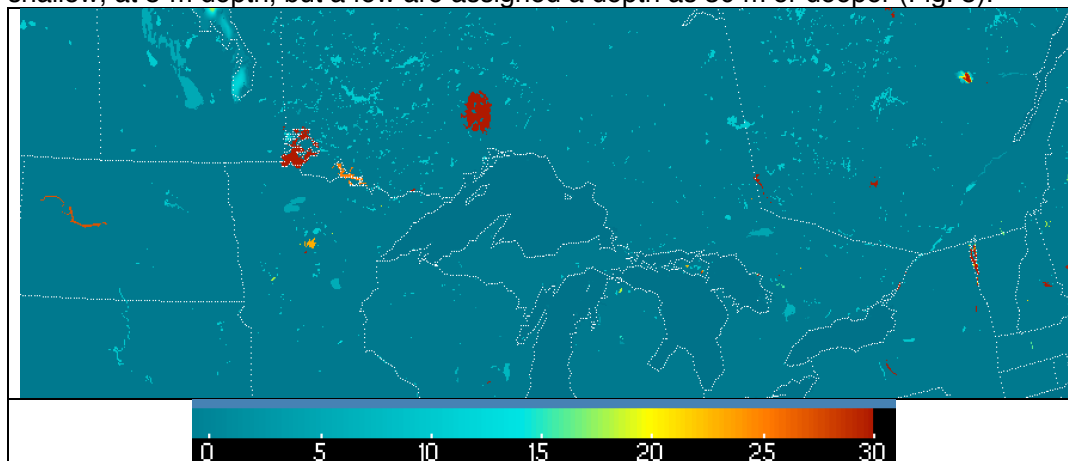
325

326

327 3.3. Lake depths

328

329 Lake depths for the HRRRv4-WRF-CLM lake configuration are assigned from a global
330 dataset provided by Kourzeneva et al (2012, hereafter K12). For some smaller lakes
331 identified using the 15" MODIS land-water mask not found in K12, a 50-m depth was
332 assumed. ECMWF applied a 25-m depth as a default depth for these small lakes
333 (Choulga et al, 2019). For many lakes in the K12 database, a single value for maximum
334 lake depth had been applied to all lake points, which results in excessive lake water
335 volume and too cold temperatures as discussed in section 5. However, the K12
336 database still allows overall differentiation between shallow and deep lakes. The
337 majority of the small lakes in the northern US and southern Canada are assigned as
338 shallow, at 5-m depth, but a few are assigned a depth as 30 m or deeper (Fig. 5).



339 *Figure 5. Lake depth for small lakes in a subset of the HRRR domain with red for lakes*
340 *30 m or deeper.*



341

342

343 3.4 Turbidity

344

345 A single value for turbidity to describe absorption of downward short-wave radiation is
346 used in CLM, allowing for a moderate amount of suspended sedimentation. Subin et al
347 (2012) describe other options for variations in radiative transfer in lake bodies to capture
348 degrees of eutrophication, but these are not used here.

349

350 3.5 Salinity

351

352 The CLM lake model is configured for fresh water. The authors manually modified the
353 freezing temperature to account for non-zero salinity (Railsback, 2006) from 0°C to -5°C
354 for Mono Lake in California and Great Salt Lake (GSL) in Utah to capture the effect of
355 salinity. Other areas of water impoundment from coastal lagoons in the 3-km HRRR
356 lake representation (Fig. 1a) also have non-zero salinity (e.g., along coasts of Gulf of
357 Mexico and Atlantic Ocean) but no change in freezing temperature is necessary for
358 these areas.

359

360 3.6 Elevation

361

362 The elevation value (above sea level) assigned to each lake grid point is the same
363 assigned to that from the atmospheric model, which may be different from reality, but at
364 least consistent with the atmospheric conditions. As mentioned earlier, the minimum
365 elevation above sea level of a grid point to be assigned as a lake is 5 m; other water
366 grid points are assumed to be ocean.

367

368 3.7 Special situations for CLM lake model application

369

370 The algorithm for the turbulent heat flux calculation in the CLM-lake model was mainly
371 based on Zenget al. (1998), except that roughness length scales for temperature and
372 humidity are the same as roughness length scale for momentum for its WRF-lake
373 application, while they are updated dynamically in CLM 4.5. Charusombat et al (2018)
374 showed that the same roughness length scales for temperature and salinity as that for
375 momentum could result in overestimated surface sensible and latent heat fluxes in
376 autumn and winter. Therefore, a revision to the CLMv4.5 lake model was introduced for
377 modified roughness lengths over water using modified formulations of the Coupled
378 Ocean-Atmosphere Response Experiment (COARE) algorithm as described by
379 Charusombat et al (2018) to improve surface sensible and latent heat fluxes.

380

381 For GSL with a very high value of salinity (270 ppt north of ~41.22°N with freezing point
382 of 249 K and 150 ppt south of ~41.22°N with freezing point at 263 K), a change of
383 freezing temperature to -5°C appeared to be not sufficient to keep the lake ice-free
384 during the cold outbreaks in winter in this high-elevation area. GSL is unusual in various



385 aspects – it is hypersaline (far more saline than the ocean), the largest terminal lake
386 (without outflow) in the Western Hemisphere (Belovsky et al, 2011), shallow (mean
387 depth of 5 m) and subject to very strong eutrophication (Belovsky et al, 2011).
388 According to GSL climatology the lake stays ice-free all winter, and its temperature goes
389 slightly below freezing only for a very short period in January and February. Thus, we
390 presume that the CLM lake model needs to allow turbidity variation (see section 3.4). A
391 solution to this representation problem was use of a bi-weekly climatology over each 1-
392 year period to bound the cycled GSL temperature at initial forecast time not to deviate
393 more than +/- 3°C from the climatological value interpolated to the current day of year.
394 Also, using special code, GSL was forced stay ice-free for the whole year as observed.
395

396 3.8 Time step

397
398 The CLM lake model within the HRRR/RAP weather models was run with the same time
399 step as for other physical processes in the HRRR model (20 s) and the RAP model (60
400 s). Again, even with this relatively high frequency for calling the CLM lake model, the
401 computational expense was extremely small, less than 0.1% of overall HRRR run time.
402

403

404 **4 Initialization for small lake temps by cycling with defined atmospheric** 405 **conditions – a strategy**

406

407 The central strategy described in this paper is to use accurate, ongoing atmospheric
408 forcing with a computationally inexpensive 1-d lake model to obtain an equilibrium state
409 of a lake temperature profile. This technique responds appropriately to strong changes
410 in atmospheric forcing (e.g., cold air outbreak or excessive heat events). With the
411 NOAA HRRR and RAP atmospheric models performing hourly data assimilation of a
412 broad set of hourly observations, accurate atmospheric forcing is available.
413

414 The RAP and HRRR hourly data assimilation cycles include these aspects, all of which
415 are important for cycling initialization of inland lakes. First, cloud assimilation (from
416 satellite and ceilometer data) to ensure accurate shortwave and longwave radiation
417 fields (Benjamin et al 2021). Second, radar reflectivity data are assimilated as part of a
418 3-km ensemble data assimilation system to ensure accurate short-range precipitation
419 (Weygandt et al, 2022, Dowell et al, 2022, James et al, 2022, Benjamin et al, 2016).
420 Finally, 2-m air temperature and moisture and 10-m wind observations are effectively
421 assimilated (i.e., producing more accurate predictions) including representation through
422 the boundary layer using pseudo-innovations (James and Benjamin, 2017). Other
423 information on the HRRR/RAP data assimilation is provided by Benjamin et al (2016).
424

425 The cycling of the 10-level CLM lake model within the experimental HRRRv4 started on
426 24 August 2018. After 10 days of cycling (Fig. 5), differences in lake temperatures
427 between HRRRv4 and the operational HRRRv3 using interpolated NSST data were

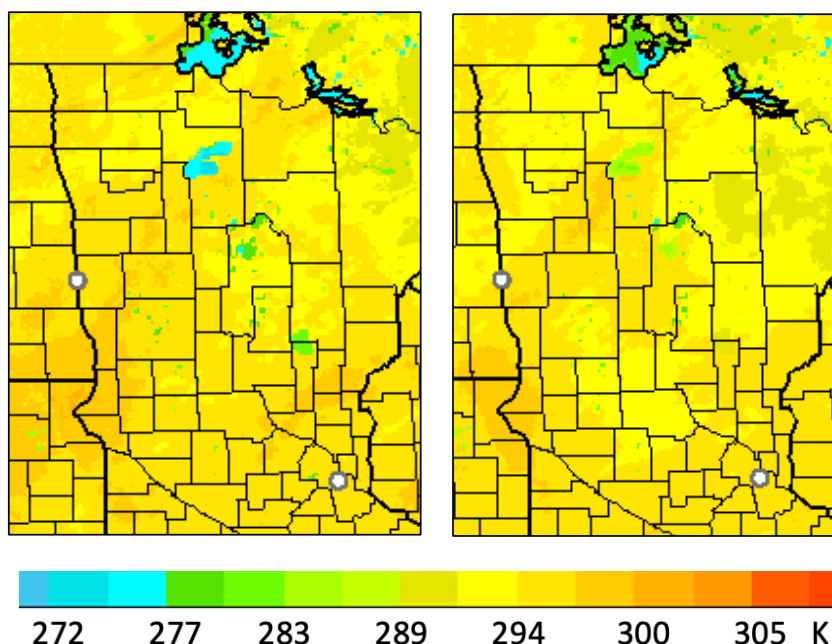


428 evident of 5-15°F (3-12°C or 276-285 K), showing that the adjustment with realistic
 429 atmospheric conditions and use of the CLM lake model with roughly accurate lake depth
 430 data was very effective.
 431

Consequences (to right) from strategy for lake initialization (below)	Coupling lake and atmosphere within initialization	Lake temps in spring-summer	Lake temps in fall
SST interpolation to small lakes	None	Much too cold, especially for shallow lakes	Still generally too cold but intermittently too warm after cold-air outbreaks.
Lake annual variation forced by reanalysis atmospheric data – 1-way cycling from atmospheric forcing	1-way	More accurate, possibly still too cold. No regime variation in a given year	More accurate, still too cold for some lakes with too-deep bathymetry data. Will not capture variation from weather regimes in a given year
2-way cycling	2-way	More accurate including yearly anomalies	More accurate including yearly anomalies

432
 433 *Table 4. Expected seasonal lake-atmosphere temperature consequences from different*
 434 *lake initialization strategies*

435
 436
 437 Possible approaches for initializing lake temperatures are summarized in Table 4. The
 438 simplest option is via larger-scale water temperature data (SST data) with horizontal
 439 interpolation to smaller water areas including inland lakes and reservoirs; this was the
 440 previous strategy for the HRRR and RAP models before introduction of cycling using
 441 the CLM lake model. An alternate strategy is to run lake models over a multi-year period
 442 forced by reanalysis atmospheric data (ERA-Interim) as described by Balsamo et al
 443 (2012), Dutra et al (2010), and Balsamo (2013) for the ECMWF to obtain a yearly
 444 varying climatology of lake temperature for all lakes represented. This method will
 445 capture the mean annual variation of lake temperatures. However, due to multi-year
 446 averaging, it cannot represent anomalous conditions in a given year (sustained heat or
 447 sustained cold conditions), which can modify temperatures especially for shallow lakes
 448 by several K within 1-2 weeks. Full cycling of the lake model within an ongoing coupled
 449 weather model, the strategy described in this paper, can represent the lingering effects
 450 of anomalously warm or cold weather upon lake temperatures and the resultant fluxes.
 451 ECMWF applies a similar ongoing cycling for lake prognostic variables (ECMWF 2020)
 452 for lake initialization.



453

454 *Figure 6. Skin temperature (K) including lake temperatures. From 18-h forecasts valid*
455 *at 15 UTC 3 September 2018 for a) operational HRRRv3 using NSST for lake*
456 *temperatures, and b) experimental HRRRv4 with CLM lake model and cycling.*

457

458 A similar challenge is initialization of lake ice cover. Similar to the treatment for lake
459 temperature, cycling of a multi-level lake model (like the CLM lake model) can provide
460 an alternative, adaptive-in-time method for lake-ice initialization. NOAA has used in the
461 HRRR and RAP the daily IMS ice cover product¹ (US National Ice Center, 2008) for
462 binary (non-fractional) lake ice cover. The IMS ice cover is used for oceans and large
463 lakes (e.g., for RAP in Fig. 1b, for Great Slave Lake and Great Bear Lake in northern
464 Canada). For small lakes below the resolution of the IMS ice map, lakes stayed open for
465 the winter before introduction of the CLM lake model with lake cycling (for grid-point-
466 specific temperature and ice cover) starting with HRRRv4 and RAPv5.

467

468

469 **5 Results**

470

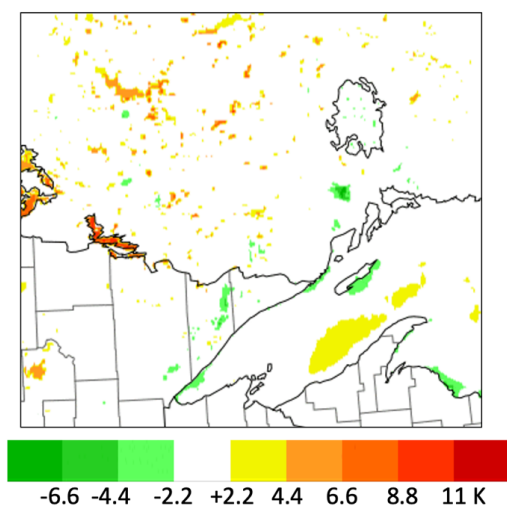
471 In this section, we describe comparisons of lake surface temperature evolution between
472 the CLM implementation described here and the lake specification through interpolation
473 from the NSST dataset (Fig. 3) at lakes in the United States and southern Canada.

474

¹ <https://usicecenter.gov/Products/ImsHome>



475 Comparisons during 2018–2019 were drawn from real-time simulations from the then-
476 operational HRRRv3 (using interpolated SST) and the experimental HRRRv4 (using
477 CLM). More recent comparisons were made for March–November 2021 between the
478 operational HRRRv4 (using CLM) and interpolated NSST values (as used in 2019–2020
479 for HRRRv3). In addition, the CLM and NSST values were compared to in situ
480 observations where available and also to satellite-based estimates defined below.
481
482
483



484
485 *Fig. 7. Difference (K) in skin temperature (including lake temperatures) between*
486 *versions of HRRR model using cycled lake-model values (HRRRv4 or HRRRX) and*
487 *using interpolated NSST data (HRRRv3 or HRRR-NCEP). Valid 1300 UTC 13 October*
488 *2019, and also includes differences from use of FVCOM lake model in HRRRv4*
489 *(Fujisaki-Manome et al, 2020).*

491 5.1 Cases from 2018 – 2019

492
493 Introduction of the CLM lake model forced by ongoing HRRRv4 atmospheric conditions
494 (i.e., cycling) allowed, within only 10 days, an increase in lake temperatures for Red
495 Lake and Lake of the Woods (both in Minnesota) from 3 K to over 10 K (Fig. 6) in
496 September 2018. A comparison in skin temperature for a year later (October 2019)
497 between versions of the HRRR model (HRRRv4 with lake cycling vs. HRRRv3)
498 including differences from with and without lake cycling is shown in Fig. 7. Higher
499 temperatures were evident for the Minnesota/Ontario lakes from cycling (vs. NSST
500 interpolation). HRRRv4 also included coupling with the 3-d FVCOM lake model for
501 the Laurentian Great Lakes, showing areas of upwelling with associated cooler water



502 over Lake Superior in Fig. 7 from predominant westerly to southwesterly near-surface
 503 wind at this time.
 504

Lake number	Lake name	State/province, country	HRRR l point	HRRR j point	Area (km ²)	Depth used (m)	Ice free?
1	Simcoe	ON, CA	1378	799		6	N
2	St. Clair	ON/MI, CA/US	1302	709	1240	6	N
3	Champlain	VT/NY, US	1534	835		77	N
4	Sebago	ME, US	1610	833		33	N
5	Okefenokee	FL, US	1459	145	1510	3	Yes
6	Pontchartrain	LA, US	1136	224	2180	10	Yes
7	Intracoastal Waterway (near Corpus Christi, TX)	TX, US	905	128	3300	10	Yes
8	Salton Sea	CA, US	337	387		9	Yes
9	Tahoe	NV/CA, US	259	628		313	N
10	Great Salt	UT, US	486	653	3050	3	Yes
11	Utah	UT, US	496	622		3	N
12	Bear	ID/UT, US	518	684		29	N
13	Sakakawea	ND, US	790	868		27	N
14	Winnebago	WI, US	1143	742		7	N
15	Lower Red	MN, US	961	880		5	N
16	Lake of the Woods	MB/MN, CA/US	965	919	3030	32	N
17	Manitoba	MB, CA	879	972	3240	5	N
18	Winnipeg	MB, CA	916	977	13270	8	N
19	Nipigon	ON, CA	956	956	5410	55	N

505 *Table 5. Lakes for comparison of lake temperatures between HRRR/CLM, NASA*
 506 *SPoRT, NSST, and in situ observations as shown in Figs. 8 and 9. Area is shown for*
 507 *lakes >1000 km². Lake depths are constant within each lake except for lakes 2, 3, and*
 508 *18. See Fig. 5 for example map of lake depth used in HRRR. Specific HRRR i/j 3-km*
 509 *grid points (indicated in table) were selected from HRRR data for each lake.*
 510

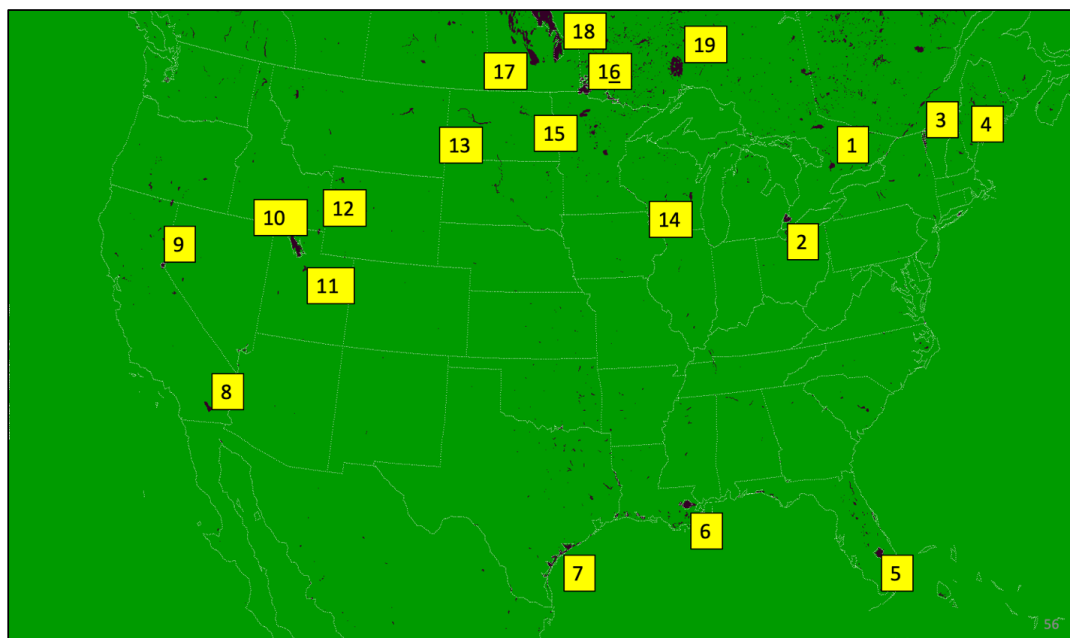


511
 512

Name of Lake	No. from Tab. 5	Source of Observation	Depth of Sensor (m)	URL
Lake St. Clair	2	ECCC	6	https://www.ndbc.noaa.gov/station_page.php?station=45147
Lake Champlain - Schuyler Reef	3	GLERL	0.45	https://www.ndbc.noaa.gov/station_page.php?station=45195
Sebago Lake @ Lower	4	Portland Water District Buoy	Est 1	https://www.pwd.org/sebago-lake-monitoring-buoy
Lake Pontchartrain @ New Canal Station	6	NOAA/ National Ocean Service	0.6	https://www.ndbc.noaa.gov/station_page.php?station=nwcl1
Intracoastal Waterway @ Baffin Bay near Padre Island	7	Texas Coastal Ocean Observing Network	unknown	https://www.ndbc.noaa.gov/station_page.php?station=babt2
Lake Tahoe	9	NASA/JPL	0.5	https://laketahoe.jpl.nasa.gov/get_imp_weather
Utah Lake @ Provo Marina	11	Utah DWQ Water Quality Network	unknown	https://wqdatalive.com/public/669
Bear Lake	12	Utah DNR State Parks	unknown	https://stateparks.utah.gov/parks/bear-lake/current-conditions/
Lake Sakakawea @ Missouri River near Williston, ND	13	USGS	unknown	https://waterdata.usgs.gov/monitoring-location/06330000/#parameterCode=00065&period=P7D

513
 514
 515

Table 6. Sources of available in situ data among 19 lakes in Table 5.



516
517

518 *Figure 8. Locations of 19 lakes (see Table 5) for lake temperature intercomparison.*
519 *These lakes are shown as mapped onto the 3-km CONUS HRRR model domain.*

520
521

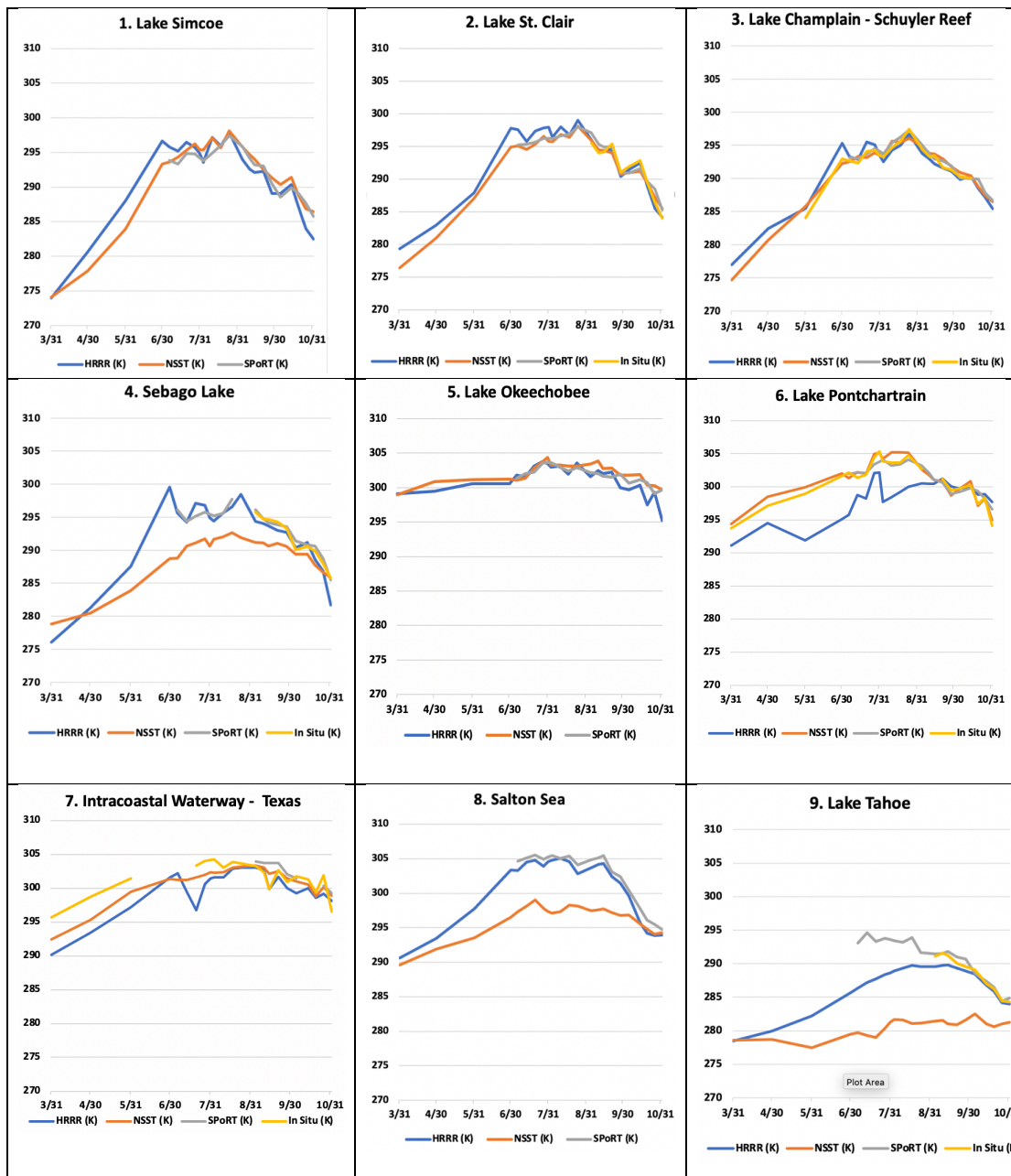
522 5.2 Comparisons of different lake temperature estimates for 19 lakes from lower 48 523 US and southern Canada during 2021.

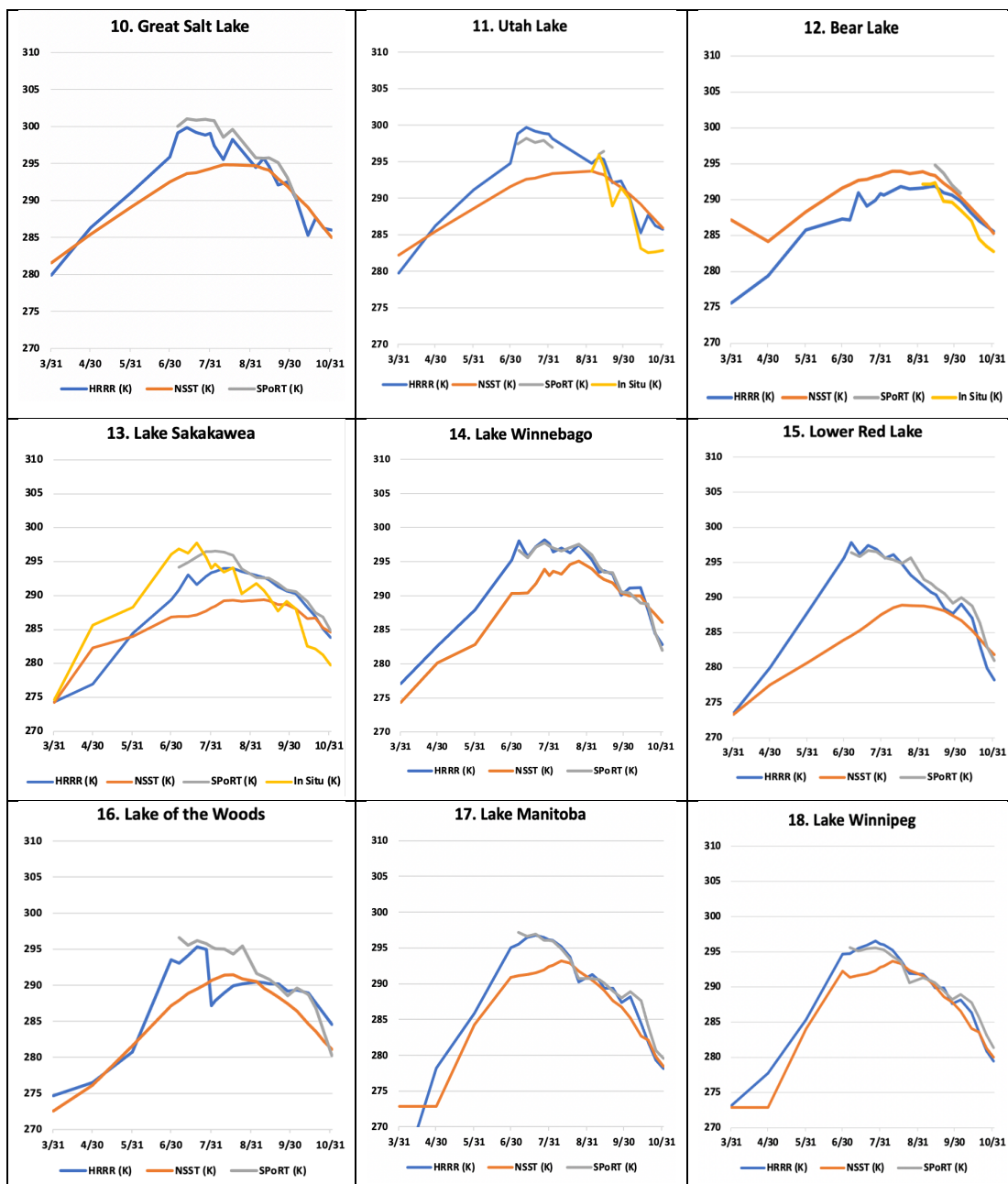
524

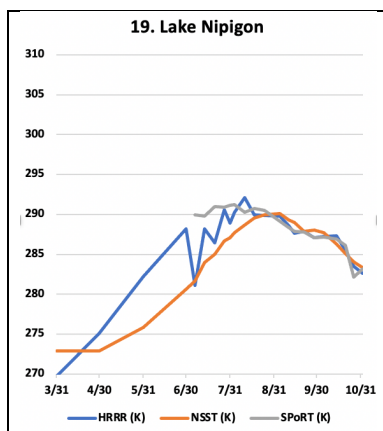
525 During a period from March to November 2021, a comparison was made of lake
526 temperatures between the cycled HRRR-CLM values and those from three other
527 estimates from NASA, NOAA, and in situ observations. A geographically diverse set of
528 19 lakes over the lower 48 United States and southern Canada was selected for these
529 comparisons as listed in Table 5 and shown in Fig. 8. Lakes selected included near-
530 ocean lagoon areas separated from ocean areas by coastal land as resolved by the 3-
531 km land-water mask as discussed in section 3.2. The water areas also included a
532 reservoir (Lake Sakakawea). Some of these lakes are dimictic or polymictic (with ice
533 cover part of each year, Lewis 1983) but five of them do not experience any ice cover
534 (Table 5), and lakes 5, 6, 7, and 8 are monomictic. The CLM lake model was cycled for
535 all these lakes in the 3-km HRRR model. The 19 lakes included seven lakes with a
536 surface area greater than 1,000 km². The March-November evaluation period include
537 the spring-summer warming period and the cooling period in autumn. Data points were
538 obtained monthly for March-August and weekly for September-November.
539
540



541







542

543 *Figure 9. Lake temperatures in 2021 (April-October) from the 19 selected lakes (Table*
544 *5, Fig. 8) from HRRR-CLM-cycled (blue), NSST (red), SPoRT (gray), in situ (orange).*

545

546

547 The HRRR-CLM values for these 19 lakes were compared with first, an estimate from
548 NASA SPoRT (Short-Term Prediction Research and Transition) real-time surface water
549 temperature composite including time-weighted MODIS and VIIRS data for inland lakes
550 (NASA, 2021, Kelley et al, 2021). The composite is valid from the surface to 2-m depth
551 and is averaged over a 7-day period to mitigate for cloud cover on a given day. A
552 second lake temperature estimate is that from NSST, as discussed earlier. Third, in situ
553 surface water temperature observations were available from observing platforms in nine
554 of the 19 lakes (Table 6). The platforms are operated by Federal, state, and local
555 government agencies and a regional ocean observing system. The depths of the water
556 temperature observations were only available at four of the nine platforms. At these four
557 sites, the depth ranged from 0.45 to 0.9 m.

558

559 In general, the HRRR-CLM-cycled lake temperatures showed the anticipated difference
560 from NSST values with quicker summer warming from HRRR-CLM cycling for all lakes
561 except the southern 3 lakes (5, 6, 7 in Table 5, with Lakes 6 and 7 essentially lagoons in
562 close proximity to the ocean) and Bear Lake in UT/ID (Lake 12, 39-m depth). The NSST
563 estimates were colder for spring through summer than HRRR values for 15 of the 19
564 lakes, a consequence from the NSST estimate via horizontal interpolation from deeper
565 bodies of water.

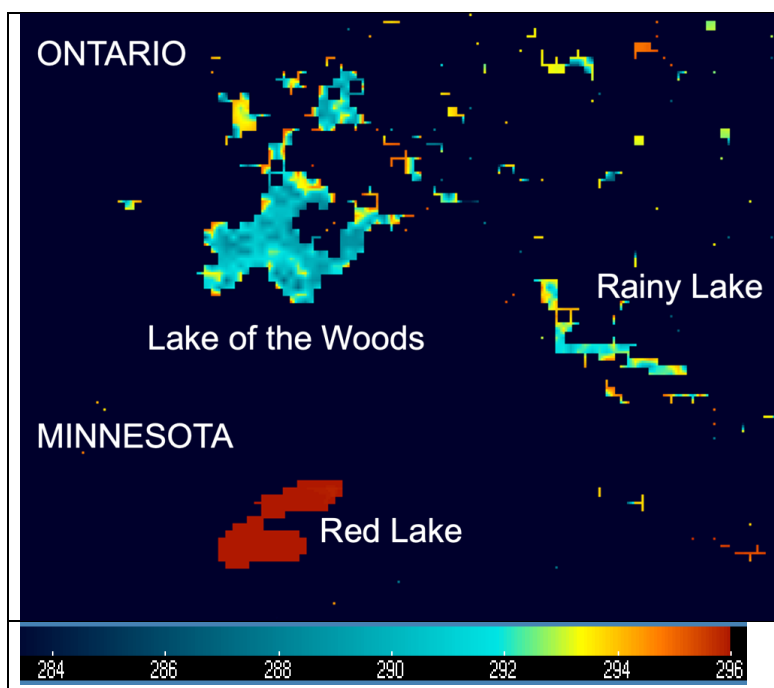
566

567 For the nine lakes with in situ observations (Table 6), the HRRR-CLM-cycled lake
568 temperatures are generally able to better capture weekly variability in summer and
569 autumn months, associated with windy periods increasing mixing or relatively warm and
570 cool weather periods or varying amounts of cloud cover. This can be seen, for
571 example, at Utah Lake and the Intracoastal Waterway west of Padre Island in Texas
572 (note cooling from passage of Hurricane Nicholas in mid-September). The most



573 dramatic improvement of HRRR-CLM over NSST lake temperatures is seen at Lake
574 Tahoe and lakes 14-19 in the northern region, with NSST estimates 5-10 K too cool. At
575 two of the lakes with in situ observations, the Intracoastal Waterway (linked to the
576 ocean) and Lake Pontchartrain, both lagoons linked to the ocean, NSST estimates are
577 generally closer than HRRR-CLM to the observations.

578
579 HRRR-CLM lake temperatures matched in situ observations well for the northern lakes,
580 usually within 1-2 K. In contrast, the lake temperature values from SPoRT were
581 generally warmer than HRRR or in situ observations in the autumn period. The SPoRT
582 observations showed a strong confirmation of HRRR-CLM-cycled lake temperatures for
583 lakes in the western US (Lakes 8-13) and most lakes in the northern areas (Lakes 4,
584 14-19). Finally, the HRRR-CLM-cycled lake temperatures during this period often
585 varied strongly from the NSST estimates, with differences of up to 5-10 K (largest
586 difference with Red Lake, Lake 15). The effect of lake depth was evident with a faster
587 transition to fully mixed lakes for shallow lakes (e.g., 5-m depth for Red Lake in MN,
588 Lake 15 in Table 5) but subject to more temporal and horizontal variation for deeper
589 lakes. Fig. 10 showed a strong intralake variation of 9 K across Lake of the Woods
590 (32-m depth) in the HRRR-CLM estimate in contrast with very little variation (< 1 K)
591 across Red Lake. Due to a lack of high-resolution observations of lake surface
592 temperatures, it is difficult to determine which intralake variations are more realistic.
593 However, we think some of these intralake contrasts from HRRR-CLM may be
594 exaggerated from actual values, possibly requiring introduction of a small temperature
595 exchange rate (diffusion) between adjacent lake columns. Differences in skin
596 temperature (e.g., SPoRT) and bulk temperature (e.g., in situ) for lakes have been
597 noted (e.g., Wilson et al, 2013) of up to 0.5 K, but the HRRR vs. NSST differences in
598 this study are generally much larger than this magnitude.
599



601 *Fig. 10. HRRR-CLM lake temperature (K) for 1500 UTC 31 July 2021 for area over*
602 *northern Minnesota (US) and southwestern Ontario (Canada).*

603
604 The main deficiencies evident so far with the HRRR-CLM lake temperatures appear to
605 be associated with errors in lake depth values. On the average, the lake depth for most
606 lakes is too deep, since the preprocessing with the K12 dataset simply assigned a
607 single lake depth value (maximum or mean) to all grid points for that lake even up to the
608 modeled lake points adjacent to land, as shown in Table 5 for 16 or the 19 lakes
609 studied. We also noted too-low lake temperatures in HRRRv4 for lake grid points at the
610 western edge of a few lakes (e.g., Tahoe, Sebago (ME), Cayuga (NY), Champlain), all
611 relatively deep lakes (Fig. 6, Table 5). We attribute this to 1-d upwelling from
612 insufficient bathymetry data resulting in cylinder-like lake volumes with constant lake
613 depths, therefore with a) too-deep lake-edge pixels coinciding with b) strong winds
614 coming off from land areas with predominantly westerly winds. This deficient effect was
615 not widespread for the HRRR model and did not affect the overall results. Again, this
616 behavior is attributed to the behavior of the lake model over integrations with the
617 inaccurate lake depth information and not to the lake cycling initialization design.

618
619

620 **6 Conclusions**

621

622 We report here on the first use of a small-lake model (CLM4.5, 10 layer) in US NOAA
623 NWP models along with an ongoing cycling of lake temperatures since 2018 to initialize



624 lake temperatures in each prediction. These models are the 3-km HRRRv4 (D22, J22)
625 and 13-km RAPv5 hourly updated models, both of which became operational in
626 December 2020 after cycling since August 2018. At 3-km grid spacing, the HRRR
627 model applied this small-lake modeling and assimilation to 1864 small lakes varying in
628 size from about 10 km² (single grid point) to 14 larger lakes over 1000 km² in surface
629 area, but not including the Laurentian Great Lakes. The effectiveness of introducing the
630 multi-layer lake model into the HRRR and RAP models was completely dependent on
631 the initialization for lake temperatures. The introduction of a cycling capability through
632 the hourly assimilation allowed the lake temperatures to evolve to accurate values,
633 consistent with recent weather. In this paper, we describe the lake cycling applied for
634 the NOAA regional 3-km HRRR and 13-km RAP weather models including the coupled
635 1-d CLM lake model. We also show some comparisons with other estimates of lake
636 temperatures. From those comparisons, the cycled lake temperatures from the 3-km
637 HRRR model were found to be reasonably accurate. HRRR lake temperatures were
638 found to be generally within 1 K of in situ observations and within 2 K of the SPoRT
639 estimates. Finally, NSST estimates of small-lake temperatures were found to often differ
640 from in situ observations and HRRR estimates by 5-12 K. Other differences between
641 lake-cycled HRRR estimates and SST-based estimates were up to 10-15 K.

642
643 From these initial results, we conclude that the lake-cycling initialization for small lakes
644 has been effective overall, owing to accurate hourly estimates of near-surface
645 temperature, moisture and winds, and shortwave and longwave estimates provided to
646 the 1-d CLM lake model every time step (20 s for 3-km HRRR model). The HRRR-CLM
647 treatment also allows some inland lakes to freeze in winter, which is more consistent
648 with observations. The lake cycling strategy is similar to that initialization method used
649 by ECMWF for its 9-km (as of 2021) IFS (Integrated Forecast System) and using a
650 binary lake mask in the 3-km HRRR model.

651
652 One deficiency noted due was development of too-cold lake surface for a few lakes on
653 their western boundary. We attribute this to the incorrect bathymetry data with constant
654 lake depth (e.g., see caption for Table 5) causing an excessive 1-d upwelling from too-
655 deep lake depth at western shores for these lakes. This issue is being addressed with a
656 current project to improve lake bathymetry data for which results will be reported in the
657 future. Also, HRRR-CLM cycling gave poorer results than NSST at least for Lake
658 Pontchartrain (Lake #6 in Table 5), suggesting to use NSST for near-ocean lagoon
659 areas. More investigation is needed for strong intralake variations overall in HRRR-
660 CLM-cycling representation (e.g., Lake of the Woods in Fig. 10) and possible
661 introduction of horizontal diffusion of temperature between adjacent lake points.

662
663 US NWS forecasters have reported much improved near-surface temperature and
664 dewpoint predictions in the vicinity of small lakes from the 3-km HRRR model in 2021
665 since the implementation of the 1-d CLM lake model and lake-cycling initialization.
666 Again, this effort complements the coupling of the HRRR model with the 3-d FVCOM
667 hydrodynamical lake model for the Laurentian Great Lakes (Fukisaki-Manome et al,



668 2020) design to improve lake-effect snow predictions. These efforts are the most
669 advanced lake-coupling and lake-initialization efforts at this point in US NOAA weather
670 models.

671
672 Overall, the improved lake temperatures from the lake cycling initialization technique
673 driven over a 3-year period by accurate atmospheric conditions described here results
674 in improved fluxes of heat and moisture over using SST interpolation and improved
675 nearby predictions of atmospheric 2-m temperature and 2-m moisture.

676 **Code availability**

677 This research used WRF version 3.9.1 including use of the option with the CLM lake
678 model. All code is available from the National Center for Atmospheric Research
679 (NCAR) at https://www2.mmm.ucar.edu/wrf/users/download/get_sources.html

680 **Data availability**

681 HRRR data are publicly available via archives hosted by Amazon Web Services
682 (<https://registry.opendata.aws/noaa-hrrr-pds/>) and Google Cloud Platform
683 (<https://console.cloud.google.com/marketplace/product/noaa-public/hrrr?project=python-232920&pli=1>).
684

685 **Author contributions**

686 SB, TS, and EJ planned the design. TS and EJ carried out the actual coding for
687 modeling, data assimilation and scripts. EJ, SB, JK, and SK extracted data from
688 experiments and other sources. EJ and JK analyzed the results. SB wrote the
689 manuscript draft and led its revision. EA, AFM, JK, GM, AG and PC (along with TS and
690 EJ) reviewed and edited the manuscript.

691 **Acknowledgments**

692 Credit is due to the WRF model team at NCAR (Jimmy Dudhia) for their help in applying
693 the CLM lake model for the HRRR and RAP applications of the WRF model. We
694 greatly appreciate our NOAA colleague, Thomas Hamill (NOAA PSL), for Fig. 4 from
695 another already published article by him. We also thank Frank J. LaFontaine and Kevin
696 K. Fuell of the NASA SPoRT Team for providing archived Northern Hemisphere SST
697 composites. Thanks also to Rob Cifelli of NOAA/PSL for a very helpful review of our
698 manuscript. This work was supported by NOAA Research base funding.

699 **References**

- 700 Anderson, E. J., Fujisaki-Manome, A., Kessler, J., Lang, G. A., Chu, P. Y., Kelley, J. G.
701 W., et al.: Ice forecasting in the next-generation Great Lakes Operational Forecast
702 System (GLOFS). *Journal of Marine Science and Engineering*, 6(123),
703 <https://doi.org/10.3390/jmse6040123>, 2018
- 704 Balsamo, G., Salgado, R., Dutra, E., Boussetta, S., Stockdale, T., Potes, M.: On the
705 contribution of lakes in predicting near-surface temperature in a global weather
706 forecasting model. *Tellus A: Dynamic Meteorology and Oceanography*.
707 <https://doi.org/10.3402/tellusa.v64i0.15829>, 2012



- 708 Balsamo, G., Interactive lakes in the Integrated Forecast System. ECMWF Newsletter
709 137, p. 30-34. [10.21957/rffv1gir](https://doi.org/10.21957/rffv1gir), 2013.
- 710
- 711 Balsamo, G., Mahfouf, J.-F.: Les schémas de surface continentale pour le suivi et la
712 prévision du système Terre au CEPMMT. *La Météorologie*, 108, 77-81, 2020.
- 713
- 714 Belovsky, G., Stephens, D., Perschon, C., et al.: The Great Salt Lake Ecosystem (Utah,
715 USA): long term data and a structural equation approach, *Ecosphere*, 2, 1-40,
716 doi.org/10.1890/ES10-00091.1, 2011.
- 717
- 718 Benjamin, S.G., D. Devenyi, S.S. Weygandt, K.J. Brundage, J.M. Brown, G. Grell, D.
719 Kim, B.E. Schwartz, T.G. Smirnova, T.L. Smith, G.S. Manikin: An hourly
720 assimilation/forecast cycle: the RUC. *Mon. Wea. Rev.*, **132**, 495-518. 2004.
- 721 Benjamin, S.G., B.D. Jamison, W.R. Moninger, S. R. Sahm, B. Schwartz, T.W.
722 Schlatter: Relative short-range forecast impact from aircraft, profiler, radiosonde, VAD,
723 GPS-PW, METAR, and mesonet observations via the RUC hourly assimilation
724 cycle. *Mon. Wea. Rev.*, **138**, 1319-1343. 2010.
- 725 Benjamin, S. G., S.S. Weygandt, M. Hu, C.A. Alexander, T.G. Smirnova, J.B. Olson,
726 J.M. Brown, E. James, D.C. Dowell, G.A. Grell, H. Lin, S.E. Peckham, T.L. Smith, W.R.
727 Moninger, G.S. Manikin: A North American hourly assimilation and model forecast
728 cycle: The Rapid Refresh. *Mon. Wea. Rev.*, **144**, 1669-
729 1694. <http://dx.doi.org/10.1175/MWR-D-15-0242.1> . 2016.
- 730 Benjamin, S.G., E.P. James, M. Hu, C.R. Alexander, T.T. Ladwig, J.M. Brown, S.S.
731 Weygandt, D.D. Turner, P. Minnis, W.L. Smith, Jr., and A. Heidinger: Stratiform cloud-
732 hydrometeor assimilation for HRRR and RAP model short-range weather prediction.
733 *Mon. Wea. Rev.*, **149**, 2673-2694. <https://doi.org/10.1175/MWR-D-20-0319.1>. 2021.
- 734 Benjamin, S.G., T.G. Smirnova, E.P. James, L.-F. Lin, M. Hu, D.D. Turner, and S. He:
735 Land-snow assimilation including a moderately coupled initialization method applied to
736 NWP. *J. Hydromet.*, 23, accepted. 2022.
- 737
- 738 Boussetta, S.; Balsamo, G.; Arduini, G.; Dutra, E.; McNorton, J.; Choulga, M.; Agustí-
739 Panareda, A.; Beljaars, A.; Wedi, N.; Munõz-Sabater, J.; de Rosnay, P.; Sandu, I.;
740 Hadade, I.; Carver, G.; Mazzetti, C.; Prudhomme, C.; Yamazaki, D.; Zsoter, E.:
741 ECLand: The ECMWF Land Surface Modelling System. *Atmosphere*, 12, 723.
742 <https://doi.org/10.3390/atmos12060723>, 2021.
- 743
- 744 Charusombat, U., Fujisaki-Manome, A., Gronewold, A. D., Lofgren, B. M., Anderson, E.
745 J., Blanken, P. D., Spence, C., Lenters, J. D., Xiao, C., Fitzpatrick, L. E., and Cutrell, G.:
746 Evaluating and improving modeled turbulent heat fluxes across the North American
747 Great Lakes, *Hydrol. Earth Syst. Sci.*, 22, 5559–5578, <https://doi.org/10.5194/hess-22-5559-2018>, 2018.
- 748



- 749
750 Chen, C., Beardsley, R. C., & Cowles, G.: An unstructured grid, finite volume coastal
751 ocean model (FVCOM) system. *Oceanography*, 19(1), 78–89.
752 <https://doi.org/10.5670/oceanog.2006.92>, 2006.
753
754 Chen, C., Beardsley, R., Cowles, G., Qi, J., Lai, Z., Gao, G., et al.: An unstructured grid,
755 Finite-Volume Coastal Ocean Model FVCOM -- User Manual. *Tech. Rep.*,
756 *SMAST/UMASSD-13-0701, Sch. for Mar. Sci. and Technol., Univ. of Mass. Dartmouth,*
757 *New Bedford.*, 416 pp., 2013
758
759 Choulga, M., Kourzeneva, E., Balsamo, G., Boussetta, S., and Wedi, N.: Upgraded
760 global mapping information for earth system modelling: an application to surface water
761 depth at the ECMWF, *Hydrol. Earth Syst. Sci.*, 23, 4051–4076,
762 <https://doi.org/10.5194/hess-23-4051-2019>, 2019.
763
764 De Pondeca, M.S.F.V., Manikin, G.S., DiMego, G., Benjamin, S.G., Parrish, D.F.,
765 Purser, R.J., Wu, W.-S., Horel, J.D., Myrick, D.T., Lin, Y., Aune, R.M., Keyser, D.,
766 Colman, B., Mann, G., and Vavra, J.: The Real-Time Mesoscale Analysis at NOAA's
767 National Centers for Environmental Prediction: Current status and development. *Wea.*
768 *Forecasting*, 26, 593-612, <https://doi.org/10.1175/WAF-D-10-05037.1>, 2011
769
770 Dirmeyer, P.A., Halder, S., Bombardi, R.: On the harvest of predictability from land
771 states in a global forecast model. *J. Geophys. Res. Atmospheres*, 123, 13,111-
772 13,127. <https://doi.org/10.1029/2018JD029103>, 2018.
773
786 Dowell, D. C., C. R. Alexander, E. P. James, S. S. Weygandt, S. G. Benjamin, G. S.
787 Manikin, B. T. Blake, J. M. Brown, J. B. Olson, M. Hu, T. G. Smirnova, T. Ladwig, J. S.
788 Kenyon, R. Ahmadov, D. D. Turner, and T. I. Alcott: The High-Resolution Rapid Refresh
789 (HRRR): An hourly updating convection-allowing forecast model. Part I: Motivation and
790 system description. *Wea. Forecasting*, accepted with revision. 2022.
791
791 Downing, J.A. et al: The global abundance and size distribution of lakes, ponds, and
792 impoundments. *Limnol. Oceanogr.*, 51, 2388-2397. 2006.
793
794 Dutra, E, Stepanenko, V. M, Balsamo, G, Viterbo, P, Miranda, P. M and co-authors: An
795 offline study of the impact of lakes on the performance of the ECMWF surface scheme.
796 *Boreal Env. Res.* 15, 100–112, 2010.
797
798 ECMWF, OpenIFS: Lakes,
799 <https://confluence.ecmwf.int/display/OIFS/3.5+OpenIFS:+Lakes>. Accessed 7 Dec 2021,
800 2020.
801
802 Fujisaki-Manome, A., G. E. Mann, E. J. Anderson, P. Y. Chu, L. E. Fitzpatrick, S. G.
803 Benjamin, E. P. James, T. G. Smirnova, C. R. Alexander, and D. M. Wright:
804 Improvements to lake-effect snow forecasts using a one-way air-lake model coupling



- 805 approach. *J. Hydrometeor.*, **21**, 2813-2828, <https://doi.org/10.1175/JHM-D-20-0079.1>,
806 2020.
807
- 808 Gao, G., C. Chen, J. Qi, and R. C. Beardsley: An unstructured-grid, finite-volume sea
809 ice model: Development, validation, and application. *J. Geophys.*
810 *Res.*, **116**, C00D04, <https://doi.org/10.1029/2010JC006688>. 2011.
811
- 812 Gemmill, W., B. Katz, and X. Li: Daily real-time, global sea surface temperature—High-
813 resolution analysis: RTG_SST_HR. NCEP Office Tech. Note 260, 39 pp. Available
814 online at <http://polar.ncep.noaa.gov/mmab/papers/tn260/MMAB260.pdf> , 2007.
815
- 816 Gu, H., Jin, J., Wu, Y., Ek, M.B., and Subin, Z.M.: Calibration and validation of lake
817 surface temperature simulations with the coupled WRF-lake model. *Climatic Change*,
818 **129**, 471-483. DOI 10.1007/s10584-013-0978-y, 2015.
819
- 820 Hamill, T.M.: Benchmarking the raw model-generated background forecast in rapidly
821 updated surface temperature analyses. Part I: Stations. *Mon. Wea. Rev.*, **148**, 689-
822 700. <https://doi.org/10.1175/MWR-D-19-0027.1>, 2020.
823
- 824 Hostetler, S.W., Bates, G., Giorgi, F.: Interactive coupling of a lake thermal model with
825 a regional climate model. *J. Geophys. Res.*, **98**, 5045-5057. DOI:[10.1029/92JD02843](https://doi.org/10.1029/92JD02843).
826 1993.
- 827 Hunter, T. S., Clites, A. H., Campbell, K. B., & Gronewold, A. D.: Development and
828 application of a monthly hydrometeorological database for the North American Great
829 Lakes - Part I: precipitation, evaporation, runoff, and air temperature. *Journal of Great*
830 *Lakes Research*, **41**(1), 65–77, 2015
- 831 James, E. P., and S. G. Benjamin: Observation system experiments with the hourly
832 updating Rapid Refresh model using GSI hybrid ensemble-variational data
833 assimilation. *Mon. Wea. Rev.*, **145**(8), 2897-2918. [https://doi.org/10.1175/MWR-D-16-](https://doi.org/10.1175/MWR-D-16-0398.1)
834 [0398.1](https://doi.org/10.1175/MWR-D-16-0398.1), 2017.
835
- 836 James, E. P., C. R. Alexander, D. C. Dowell, S. S. Weygandt, S. G. Benjamin, G. S.
837 Manikin, J. M. Brown, J. B. Olson, M. Hu, T. G. Smirnova, T. Ladwig, J. S. Kenyon, and
838 D. D. Turner: The High-Resolution Rapid Refresh (HRRR): An hourly updating
839 convection-allowing forecast model. Part II: Forecast performance. *Wea. Forecasting.*,
840 accepted with revision, 2022.
841
- 842 Kelley, S.G.T, J.G.W. Kelley, and E.J. Anderson: Evaluation of the NASA SPoRT
843 Composite Product of surface water temperatures for large lakes in New England and
844 New York State. *Abstract, 24th Conference on Satellite Meteorology, Oceanography,*
845 *and Climatology*. Available at
846 <https://ams.confex.com/ams/101ANNUAL/meetingapp.cgi/Paper/381301>, 2021.
847



- 848 Kourzeneva, E., Asensio, H., Martin, E., Faroux: Global gridded dataset of lake
849 coverage and lake depth for use in numerical weather prediction and climate modelling.
850 *Tellus A.*, 64: 15640. 10.3402/tellusa.v64i0.15640, 2012.
851
- 852 Lawrence, D. M., Fisher, R. A., Koven, C. D., Oleson, K. W., Swenson, S. C., Bonan,
853 G., et al.: The Community Land Model version 5: Description of new features,
854 benchmarking, and impact of forcing uncertainty. *Journal of Advances in Modeling Earth*
855 *Systems*, 11, 4245-4287. <https://doi.org/10.1029/2018MS001583>, 2019.
856
- 857 Lewis, W. M., Jr.: A revised classification of lakes based on mixing. *Can. J. Fish.*
858 *Aquat. Sci.* 40, 1779-1787. <https://doi.org/10.1139/f83-207>, 1983
859
- 860 Mallard, M.S., Nolte, C.G., Spero, T.L., Bullock, O.R., Alapaty, K., Herwehe, J.A., Gula,
861 J., Bowden, J.H.: Technical challenges and solutions in representing lakes when using
862 WRF in downscaling applications. *Geosci. Model Dev.*, 8, 1085-1096, 2015.
863
- 864 Mironov, D., Heise, E., Kourzeneva, E., Ritter, B., Schneider, N., and Terzhevik, A.:
865 Implementation of the lake parameterisation scheme FLake into numerical weather
866 prediction model COSMO, *Boreal Environ. Res.*, 15, 218–230, 2010.
867
- 868 Muñoz-Sabater, J., H. Lawrence, C. Albergel, P. de Rosnay, L. Isaksen, S.
869 Mecklenburg, Y. Kerr, and M. Drusch: Assimilation of SMOS brightness temperatures in
870 the ECMWF Integrated Forecasting System. *Quart. J. Roy. Meteor. Soc.*, **145**, 2524–
871 2548, <https://doi.org/10.1002/QJ.3577> , 2019.
872
- 873 NASA: Surface water temperature composite.
874 <https://weather.msfc.nasa.gov/sport/sst/>. Downloaded 2 Nov 2021, 2021
- 875 National Weather Service: Service Change Notice 20-10. Available at
876 https://www.weather.gov/media/notification/scn20-10nsst1_0.pdf , 2020.
- 877 Pondeva, M.S.F.V. de, G.S. Manikin, G. DiMego, S.G. Benjamin, D.F. Parrish, R.J.
878 Purser, W.-S. Wu, J. Horel, Y. Lin, R.M. Aune, D. Keyser, L. Anderson, B. Colman, G.
879 Mann, and J. Vavra: The Real-Time Mesoscale Analysis at NOAA's National Centers for
880 Environmental Prediction: Current Status and Development. *Wea. Forecasting*, **26**, 593-
881 612. 2011.
- 882 Railsback, B.: Some fundamentals of mineralogy and geochemistry. Figure on lake
883 salinity at <http://railsback.org/Fundamentals/SFMGLakeSize&Salinity071.pdf>, 2006
884
- 885 Skamarock, W. C., and Coauthors, 2019: A description of the Advanced Research WRF
886 version 4. NCAR Tech. Note NCAR/TN-556+STR, 162 pp., [Available online at
887 http://www2.mmm.ucar.edu/wrf/users/docs/technote/v4_technote.pdf]. 2019.
888



- 889 Subin, Z. M., Riley, W. J., & Mironov, D.: An improved lake model for climate
890 simulations: Model structure, evaluation, and sensitivity analyses in CESM1. *Journal of*
891 *Advances in Modeling Earth Systems*, 4(1). <https://doi.org/10.1029/2011ms000072>,
892 2012.
893
- 894 Thiery, W., Stepanenko, V., Fang, X., Jöhnk, D., Li, Z., Martynov, A., Perroud, M.,
895 Subin, Z., Darchambeau, F., Mironov, D., Van Lipzig, N.: LakeMIP Kivu: evaluating the
896 representation of a large, deep tropical lake by a set of one-dimensional lake models,
897 *Tellus A: Dynamic Meteorology and Oceanography*, 66:1, 21390, DOI:
898 10.3402/tellusa.v66.21390, 2014.
899
- 900 U.S. National Ice Center, updated daily: *IMS Daily Northern Hemisphere Snow and Ice*
901 *Analysis at 1 km, 4 km, and 24 km Resolutions, Version 1*. Boulder, Colorado USA.
902 NSIDC: National Snow and Ice Data Center.
903 doi: <https://doi.org/10.7265/N52R3PMC>. Accessed 8 November 2021, 2021.
904
- 905 Vanderkelen, I., van Lipzig, N. P. M., Sacks, W. J., Lawrence, D. M., Clark, M.,
906 Mizukami, N., Pokhrel, Y., and Thiery, W.: The impact of global reservoir expansion on
907 the present-day climate, EGU General Assembly 2021, online, 19–30 Apr 2021,
908 EGU21-723, <https://doi.org/10.5194/egusphere-egu21-723>, 2021
909
- 910 Verpoorter, C., Kutser, T., Seekell, D.A., and Tranvik. L.J.: A global inventory of lakes
911 based on high-resolution satellite imagery. *Geophys. Res. Lett.*, 41, 6396–6402,
912 doi:10.1002/2014GL060641. 2014.
913
- 914 Wang, F., Ni, G., Riley, W. J., Tang, J., Zhu, D., and Sun, T.: Evaluation of the WRF
915 lake module (v1.0) and its improvements at a deep reservoir, *Geosci. Model Dev.*, 12,
916 2119–2138, <https://doi.org/10.5194/gmd-12-2119-2019>, 2019.
917
- 918 Weygandt, S. S., S. G. Benjamin, M. Hu, C. R. Alexander, T. G. Smirnova, and E. P.
919 James: Radar reflectivity-based model initialization using specified latent heating
920 (Radar-LHI) within a diabatic digital filter or pre-forecast integration. *Wea. Forecasting*,
921 accepted with revision, 2022.
922
- 923 Wilson, R. C., Hook, S. J., Schneider, P., and Schladow, S. G.: Skin and bulk
924 temperature difference at Lake Tahoe: A case study on lake skin effect. *J. Geophys.*
925 *Res. Atmos.*, 118, 10,332-10,346, <https://doi.org/10.1002/jgrd.50786>, 2013.